33RD INTERNATIONAL COSMIC RAY CONFERENCE, RIO DE JANEIRO 2013
THE ASTROPARTICLE PHYSICS CONFERENCE

Shaping the gamma-ray pulsar profiles: caustic effects versus intrinsic emissivity

J. DYKS, B. RUDAK

Nicolaus Copernicus Astronomical Center, Rabiańska 8, 87-100, Toruń

jinx@ncac.torun.pl

Abstract: Gamma-ray pulsar profiles are widely believed to be dominated by caustic effects. The caustic pile-up of photons at a preferred pulse phase can be understood in two equivalent ways: either as a result of aberration and retardation effects, or simply as emission from regions where the curvature of electron trajectories in the inertial observer frame is minimum. For the curvature radiation mechanism, the vanishing curvature in the caustic regions can strongly affect the shape of modelled profiles. We calculate this effect for several generic models of gamma-ray emission, considering the impact of extended accelerating electric fields, electron energy distributions and emission region geometry. We find that slot-gap-like models with curvature emission usually do not produce the caustic-dominated profiles. The outer gap model, on the other hand is much less sensitive to the effects of curvature and usually preserves the caustic-style profile shapes.

Keywords: pulsars, gamma-rays, non-thermal radiation processes.

1 The equivalence of caustic effects and trajectory straightening

The caustic effects in rotating pulsar magnetosphere are equivalent to the straightening of electron trajectory which is traced in the inertial observer frame (IOF). A specially simple case that allows us to prove this, is the near-dipole-axis emission within the plane of rotational equator, for a pulsar with orthogonal dipole inclination $\alpha = 90^\circ$. The curvature radius of electron trajectory in IOF can be written as

$$\rho \approx c^2/|\vec{a}_{\rm iof}|, \qquad (1)$$

where $\vec{a}_{\rm iof}$ is the electron acceleration in the IOF, and c – the speed of light – is the approximate velocity of the high-energy electrons. The IOF acceleration can be expressed as a sum of two vectors:

$$\vec{a}_{\rm iof} = \vec{a}_B + \vec{a}_\Omega \approx (c^2/\rho_B)\hat{\rho}_B + 2\Omega c\hat{e}_\phi, \qquad (2)$$

where $\vec{a}_B$ is the corotating frame (CF) acceleration caused by the curvature of B-field lines and $\vec{a}_\Omega$ is the acceleration generated by the corotation, in the case of bound motion along $\vec{B}$ in the CF, see Dyks 2008). The symbol ρ_B represents the radius of curvature of B-field lines in the CF: $\rho_B \approx (4/3)s^{-1}(r/R_{\rm lc})^{1/2}$, $\hat{\rho}_B$ (with a hat) is a unit vector along that radius of curvature, $\hat{e}_\phi$ is the local azimuthal vector of unit length, and s is the footprint parameter ($s = 0$ at the magnetic pole, $s = 1$ at the rim of polar cap). In the small-angle approximation, on the trailing side of dipole axis $\hat{\rho}_B \approx -\hat{e}_\phi$, hence the IOF radius of curvature is:

$$\rho = R_{\rm lc}\left|\frac{3}{4}\frac{s}{\sqrt{r/R_{\rm lc}}} - 2\right|^{-1} = R_{\rm lc}\left|\frac{R_{\rm lc}}{\rho_B} - 2\right|^{-1} \qquad (3)$$

(trailing side). One can see that ρ can explode to infinity in the caustic regions, ie. wherever $\rho_B = R_{\rm lc}/2$.

The standard view of caustic peaks' formation, is that the detection phase of photons emitted at different radial distances r, becomes stabilised (temporarily fixed and r-independent), because the aberration and retardation counterbalance the effect of backward curvature of B-field lines. In the CF the radiation from position $\vec{r}$ in dipolar magnetic field is emitted at the angle $\theta_b \approx (3/2)s\sqrt{r/R_{\rm lc}}$ with respect to the dipole axis $\vec{\mu}$. The pulse phase of detection of this radiation is advanced by $r/R_{\rm lc}$ by the aberration of photon propagation direction between the CF and IOF frames. Since the emission point at $\vec{r}$ is closer to the observer than the center of the neutron star, the detection phase is furthermore advanced by the propagation-time-related angle $r/R_{\rm lc}$. The radiation emitted at the trailing side of the dipole axis is therefore detected at the phase:

$$\phi \approx (3/2)s\sqrt{r/R_{\rm lc}} - 2r/R_{\rm lc} + \phi_{\rm f}, \qquad (4)$$

where $\phi_{\rm f}$ is the fiducial phase which marks the detection of $r = 0$ emission along the dipole axis. The caustic effects appear when the detection phase stops increasing despite

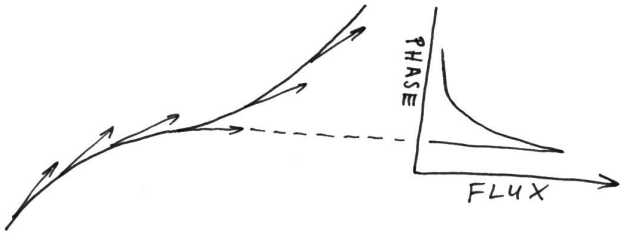

Fig. 1: The principle of creation of caustic peaks in pulsar lightcurves, as described purely in the reference frame of the inertial observer, ie. with no reference to aberration and retardation. The arrows tangent to the electron trajectory (left) mark directions of photon emission. The sharp spikes in flux correspond to the minimum curvature of electron trajectory in IOF. For layout reasons, the flux in the right-hand-side plot is marked on the horizontal axis, pulse phase on the vertical.

increasing r. This is ensured by the condition $d\phi/dr = 0$, where, from eqs. (4) and (3):

$$\left|\frac{d\phi}{dr}\right| = \frac{1}{R_{\rm lc}}\left|\frac{3}{4}\frac{s}{\sqrt{r/R_{\rm lc}}} - 2\right| = \frac{1}{\rho}. \qquad (5)$$

Eq. (5) tells us that the condition for the caustic freezing of detection phase ($d\phi/dr = 0$) is the same as the condition for the vanishing curvature of electron trajectory in the IOF ($\rho = \infty$) (Dyks, Wright & Demorest 2010; for a more general formulation of the caustics see eq. 15 in Bai & Spitkovsky 2010, hereafter BS10).

1.1 Caustics and emissivity

To estimate how important for the profile shape the vanishing curvature can be, we assume that the peak flux F of a gamma-ray peak is proportional to the range Δr of radial distances that contribute to it, and to the intrinsic emissivity $\eta(\nu,\gamma,\rho)$. The caustic effects squeeze the profile in one (azimuthal) direction only, therefore, the flux is inversely proportional to $|\Delta\phi|$:

$$F(\phi) \propto \frac{\eta\Delta r}{|\Delta\phi|} = \eta\rho. \qquad (6)$$

where the right-hand side equality is based on $\Delta\phi = \Delta r/\rho$ (eq. 5). For the uniform emissivity ($\eta = 1$ in eq. 6), which is widely used in profile atlases, the spikiness of peaks is proportional to ρ. However, for the curvature radiation (CR), the emissivity decreases with decreasing curvature. At low frequencies $\nu \ll \nu_{\rm cr}$, one has $\eta(\nu) \propto \rho^{-2/3}$, whereas at the spectral peak $\nu \sim \nu_{\rm cr}$ (and above) η drops down sharply, because the exponential cut-off moves towards low frequencies with increasing ρ. In the low-ν limit of $\nu \ll \nu_{\rm cr}$, ie. in the case of the least sensitive dependence on ρ, the flux in gamma-ray peaks becomes: $F \propto \rho^{1/3}$. Thus, the ρ-dependence of curvature emissivity is able to cancel at least two-thirds of the caustic effects that are observed in the uniform-emissivity case. and the cancellation of the caustic effects is expected to be even stronger at high ν.

2 Numerical results

We use the 3D geometrical code described in Dyks, Harding & Rudak (2004, hereafter DHR04) with the refinements of BS10. In DHR04 the emissivity was proportional to the CF value of the step length ds_{CF} of electron trajectory, and a transformation of $\vec{B}$ field between the CF and IOF was missing. This was considered reasonable because other neglected effects, such as the longitudinal currents were capable to modify $\vec{B}$ by a larger factor ($\beta^{3/2}$, where $v = \beta c$ is the local corotation velocity) than the second-order transformations that we ignored ($\sim \beta^2$). However, numerical calculation shows that both the transformation of ds and the transformation of $\vec{B}$ change the profile shape by a similar, and noticeable magnitude (Fig. 2). Moreover, they work in the same direction, and together can considerably (qualitatively) influence a profile. Fig. 2, calculated for the same parameters as fig. 5g in DHR04, shows that the transformation of ds and $\vec{B}$ can inverse the flux ratio of peaks of different origin. With the transformations included, the outer gap (OG) leading peak (at $\phi = 0.17$) becomes much stronger than the leading peak of two-pole-caustic (TPC) model (at $\phi = 0.1$). The opposite is true for the trailing peak (the TPC peak overpowers the OG peak). Generally, the refinements enhance the outer-magnetospheric emission with respect to the low-altitude one.

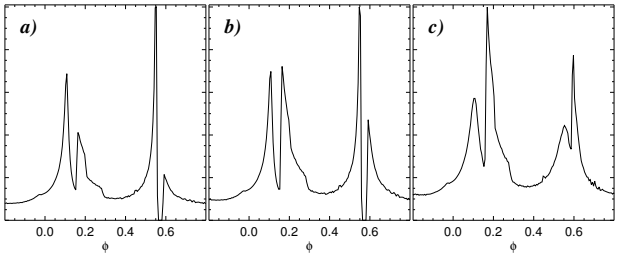

Fig. 2: The influence of second-order model refinements on the modelled lightcurves for dipole tilt $\alpha = 60^\circ$ and viewing angle $\zeta = 70^\circ$. In a) the emissivity η is proportional to the CF step length ds_{CF} and transformation of $\vec{B}$ between the IOF and CF is neglected. In b) the value of η is proportional to the IOF value of ds instead of ds_{CF}. In c) the B-field is transformed properly and the IOF value of ds is used. Note that both effects decrease the importance of the leading TPC peak ($\phi = 0.1$) with respect to the leading peak of the outer gap ($\phi = 0.17$).

2.1 Curvature radiation with a fixed maximum Lorentz factor

To assess the interplay between the caustic effects and intrinsic curvature emissivity, we first consider the CR from primary electrons with artificially fixed (r-independent) Lorentz factor of $\gamma = 10^7$. Unlike in Fig. 2, the emission region (gap) now has a non-zero transverse width. Emission is traced for B-field lines with the open-volume transverse coordinate $r_{\rm ov}$ between 0.95 and 1.05, with a gaussian profile normalisation imposed in the transverse direction ($\sigma_{\rm ov} = 0.025$, cf. eq. 1 in DHR04). The radial profile of emissivity is that of the CR for the IOF values of ds and ρ. The maximum axial distance from the rotation axis is limited to $r_{\rm max} = 0.5R_{\rm lc}$ to avoid the overlap of the TPC and OG emission patterns (this is dictated solely by the space limitations of this paper, and allows us to simultaneously assess the lightcurve shapes for both models from a single figure).

Fig. 3a shows the resulting lightcurve at the photon energy $\varepsilon = 100$ MeV which is in the $\nu \ll \nu_{\rm cr}$ regime. As estimated in section 1.1, the caustic peaks are much less pronounced, with the OG part of the profile ($\phi \in (0.3, 0.5)$) resembling a rectangle, and the TPC leading peak (at $\phi \approx 0.13$) is strongly reduced in comparison to the low-altitude emission from the polar-cap vicinity around $\phi = 0$. For even higher photon energy ($\varepsilon = 10$ GeV, Fig. 3b) the curvature radii in the caustic regions are too large for the curvature spectrum to reach the band. The profile consists of only the low-altitude emission from a region close to the polar cap, where ρ is the smallest one.

Fig. 3c is for the CR emitted by the electron energy distribution $N_e \propto \gamma^{-4}$ extending up to $\gamma = 10^7$. Although we show the profile for $\varepsilon = 100$ MeV, the result is practically the same for any energy in the range 100 MeV $\lesssim \varepsilon \lesssim$ a few GeV. Above a few GeV the profile becomes similar to the one shown in Fig. 3b. It can be seen that in none of the cases shown in Fig. 3 are the profiles dominated by the

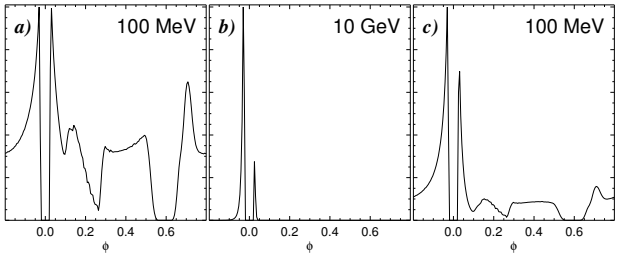

Fig. 3: Modelled lightcurves for $\alpha = 60^\circ$ and $\zeta = 60^\circ$. The emissivity of CR for the IOF values of ds and ρ is used. In a) and b) the Lorentz factor was fixed at $\gamma = 10^7$ everywhere in the magnetosphere. In c), the electron energy distribution of $N_e \propto \gamma^{-4}$ was used. The profiles refer to the photon energy shown in the top-right corner of each panel.

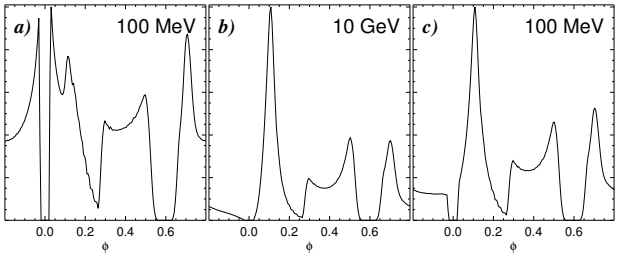

Fig. 4: Modelled lightcurves for the radiation-reaction-limited acceleration. In a) and b) the r-dependent Lorentz factor was equal to $\gamma = \gamma_{\rm eq}$ everywhere in the magnetosphere. In c), we have used the electron energy distribution $N_e \propto \gamma^{-4}$ extending up to $\gamma_{\rm eq}$. The other parameters are the same as in the previous figure.

caustic peaks. This is also true for other viewing angles, for the lack of space not illustrated here.

2.2 Curvature radiation in the case of spatially-extended acceleration

In the case of radiation-reaction-limited acceleration, the energy-loss caused by the CR: $d\gamma/ds = -2e^2(3mc)^{-1}\gamma^4\rho^{-2}$ is compensated by the energy gain provided by the electric field: $d\gamma/ds = eE_\parallel/(mc^2)$. The electrons then reach the equilibrium Lorentz factor $\gamma_{\rm eq} = 236 E_\parallel^{1/4}\rho^{1/2}$, where $E_\parallel$ is in esu and ρ in cm. Since $\gamma_{\rm eq} \propto \rho^{1/2}$, the influence of the caustic decrease of curvature may now have an opposite effect on the profiles. However, the ρ-dependence of γ affects exclusively the high-energy end of the CR spectrum (the peak and the exponential cutoff), which is the only part that is sensitive to γ. Thus, the smaller is the curvature, the more energetic become the electrons, and the larger is the gamma-ray flux at the spectral end.

To keep the conditions maximally simple, we assume a spatially uniform value of the electric field: $E_\parallel = w^2\Delta V_{\rm pc}/R_{\rm lc}$ (Hirotani 2013), where $\Delta V_{\rm pc}$ is the cross-cap potential drop and w is the gap width in units of the transverse radius of the open volume (in this paper we take $w = 0.1$, $B_{\rm pc} = 6$ TG, and $P = 33$ ms). The potential drop is scaled by the light cylinder radius $R_{\rm lc}$ to obtain a weak electric field of the outer magnetosphere. The results shown in Fig. 4 have been obtained for the Lorentz factor γ set equal to $\gamma_{\rm eq}$ at each point along the electron trajectory.

Fig. 4b shows that indeed, in the presence of extended accelerating field, the profiles do assume their normal caustic look at the high-energy end of the spectrum ($\varepsilon \gtrsim$ a few GeV). However, the low-energy part of the CR spectrum ($\nu \ll \nu_{\rm cr}$) is mostly independent of γ and retains its usual dependence on ρ ($\eta \propto \rho^{-2/3}$), ie. the flux below the spectral peak decreases with the caustic increase of ρ. Therefore, the caustic look of profiles does not prevail within the entire high-energy range: at hundreds of MeV the caustic peaks diminish considerably in comparison to the low-r emission near $\phi = 0$ (Fig. 4a). Thus, it is found that even in the case of the extended acceleration, and the favourable dependence of $\gamma_{\rm eq}$ on ρ, the profiles do not follow the caustic shapes within the full high-energy range.

Fig. 4c presents the extended aceleration case for the power-law electron energy spectrum ($N_e \propto \gamma^{-4}$ for $\gamma \leq \gamma_{\rm eq}$). In this artificial case the profiles assume the same caustic-dominated form regardless of photon energy. This

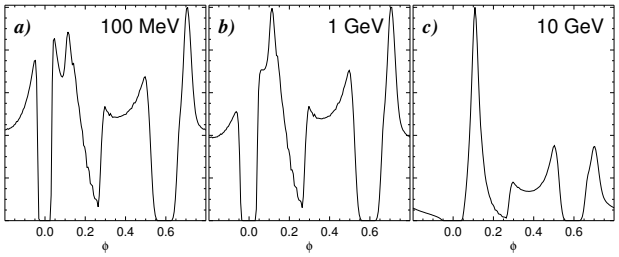

Fig. 5: Modelled lightcurves at photon energies $\varepsilon = 0.1$, 1, and 10 GeV (left to right) for the case of the spatially-extended acceleration. All panels are for the monoenergetic electrons with the Lorentz factor resulting from acceleration by the uniform electric field $E_\parallel$. Near the surface ($\phi \sim 0$) the electrons had $\gamma \ll \gamma_{\rm eq}$. The other parameters are the same as in the previous figure.

is the only case for which the CR is able to produce the caustic-style profiles throughout the entire high-energy range. However, the physical conditions that are required for this are self-inconsistent: the presence of the electric field must tend to accelerate all particles up to $\gamma_{\rm eq}$ and makes it difficult to create the wide electron energy distribution.

The difficulty in producing the caustic-peak-dominated profiles is a problem for slot-gap-like models, which include the low-altitude emission. The outer gap, on the other hand, is much less sensitive to the physics of emission process (cf. the phase range between 0.3 and 0.6 in different figures).

The electric field of the outer magnetosphere is relatively weak: $E_\parallel = 1.3\ 10^5$ esu $w^2 B_{12}(R_6/P_{33})^3$, where $R_{NS} = R_6 \cdot 10^6$ cm is the neutron star radius, B_{12} is the polar magnetic field in TG, and $P = P_{33} \cdot 33$ ms is the pulsar rotation period. The length-scale of electron acceleration up to $\gamma_{\rm eq}$ is equal to $c\tau_{\rm acc} = 1704$ cm $\gamma/E_\parallel$[esu] and can reach several R_{NS}. For this reason, an electron, which starts from the surface with $\gamma \sim 1$, at low altitudes has $\gamma \ll \gamma_{\rm eq}$ and is incapable of contributing to the gamma-ray band. As shown in Fig. 5, this can produce noticeable effects in the lightcurves (suppression of emission near $\phi = 0$). In Fig. 5, the electrons have been accelerated from $\gamma = 2$ at the surface by the same uniform electric field as before. The magnitude of the suppression can be assessed from the comparison of panels a) in Figs. 4 and 5. Around 1 GeV, where the caustic peaks start to dominate over the low-r emission, the low-

γ initial acceleration phase is able to completely remove the low-r peaks near $\phi = 0$ (Fig. 5b, to be compared with 5a). This is a way in which slot-gap-like models can get rid of the low-altitude near-polar-cap emission, provided it is possible to justify electric fields weaker than $0.01\Delta V_{\rm pc}/R_{\rm lc}$ in the low-altitude region.

The accelerating electric field can also have an opposite effect of increasing the actual value of γ above the equilibrium value $\gamma_{\rm eq}$. This is possible in the caustic regions, where the curvature, and so the CR cooling, can almost disappear. This opens the possibility for γ to overshoot $\gamma_{\rm eq}$ because of the temporarily unbalanced acceleration. Such an effect is expected to be the strongest for motion near the rotational equator of pulsars with large dipole inclinations, and for electrons moving within the closed field line region ($r_{\rm ov} \leq 1$). Numerical tests with the electric field used in this paper ($w = 0.1$, $B_{12} = 6$, $P = 33$ ms), have shown that the overshooting is weak, and the biggest difference we have noted was $\gamma = 1.17\gamma_{\rm eq}$.

3 Other emission mechanisms

The CR is successful in reproducing the high-energy spectrum of selected objects (eg. the Vela pulsar, fig. 4 in Rudak et al. 2002), however, if it is the only process considered, it may have difficulties in reproducing spectral properties of most of the other gamma-ray pulsars. Therefore, it is interesting to consider if other emission mechanisms, different from the curvature radiation, may be capable of providing us with the uniform emissivity that generates the caustic-type profiles.

The synchrocurvature emission from electrons gyrating at small pitch angles can be considered as a potentially uniformly emitting mechanism. However, in this case the radiative cooling rate will be dependent on the local curvature of the gyration trajectory. Therefore, the advantage of the increased emissivity from caustic regions may be unavailable, because it is the caustically-decreased *global* curvature, which allows for the accelerated electrons to reach higher energies thanks to the smaller radiative cooling (Fig. 4b). Moreover, calculations such as shown in fig. 2 of Harding, Usov & Muslimov (2005) suggest that the pitch angle and electron energy can change considerably with r, and make the emissivity nonuniform.

In the case of the inverse Compton scattering (ICS) it may be difficult to have emission that is uniform in magnetic mazimuth, especially for fast-rotating pulsars with large dipole inclination, which are also known to possess the caustic-like profiles (Abdo et al. 2013). This is because the electrons outflowing on the trailing side of the open volume move approximately radially outward, and roughly parallel to seed photons, regardless of whether they have thermal or nonthermal origin (Fig. 6). The electrons on the leading side can collide with the photons at much larger angles, hence the ICS emission on the leading side is expected to be much stronger.

Acknowledgment: This work was supported by the National Science Centre grant DEC-2011/02/A/ST9/00256.

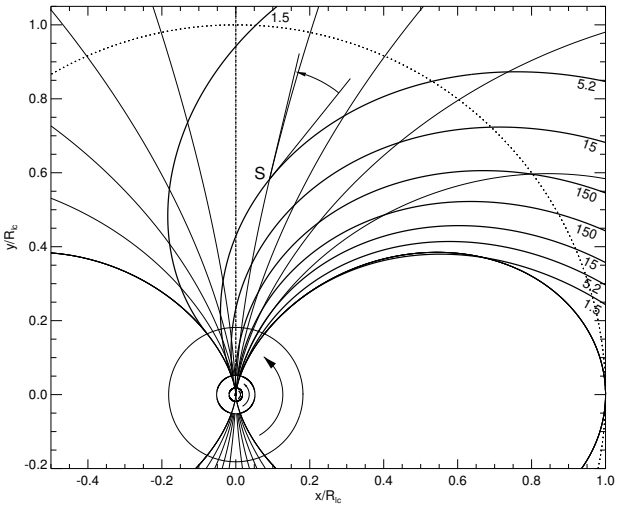

Fig. 6: Trajectories of photons, emitted from the leading and trailing sides of the polar cap, in the corotating reference frame (thick solid). Thin solid curves present the dipolar B-field lines, ie. the trajectories of electrons in the same frame (CF). The leading-side photons collide with the electrons at larger angles than on the trailing side. The numbers give the rotation period P in ms, the dotted circle marks the light cylinder, and the neutron stars centered at $(x,y) = (0,0)$ are appropriately scaled with respect to $R_{\rm lc}$.

References

[1] A.A. Abdo et al. (The Fermi-LAT collaboration), submitted to The Astrophysical Journal Supplement (2013) (astro-ph/1305.4385)
[2] X.-N. Bai and A. Spitkovsky, The Astrophysical Journal 715 (2010) 1270-1281 doi:10.1088/0004-637X/715/2/1270
[3] J. Dyks, Monthly Notices of the Royal Astronomical Society 391 (2008) 859-868 doi:10.1111/j.1365-2966.2008.13923.x.
[4] J. Dyks, A.K. Harding and B. Rudak, The Astrophysical Journal, 606 (2004) 1125-1142 doi:10.1086/383121 (DHR04)
[5] J. Dyks, G.A.E. Wright, P. Demorest, Monthly Notices of the Royal Astronomical Society 405 (2010) 509-519 doi:10.1111/j.1365-2966.2010.16462.x
[6] A.K. Harding, V.V. Usov and A. Muslimov, The Astrophysical Journal 622 (2005) 531-543 doi:10.1086/427840.
[7] K. Hirotani, The Astrophysical Journal 766 (2013) 98-107 doi:10.1088/0004-637X/766/2/98
[8] B. Rudak, J. Dyks and T. Bulik, MPE Report 278 (2002) 142-155